Phase relations in peridotitic and pyroxenitic rocks in the model systems CMASH and NCMASH

Article *in* Journal of Petrology · January 2000

DOI: 10.1093/petrology/41.1.69 · Source: OAI

1 author:

Esther Schmädicke
Friedrich-Alexander-University of Erlangen-Nürnberg
52 PUBLICATIONS **1,220** CITATIONS

JOURNAL OF PETROLOGY | VOLUME 41 | NUMBER 1 | PAGES 69–86 | 2000

Phase Relations in Peridotitic and Pyroxenitic Rocks in the Model Systems CMASH and NCMASH

ESTHER SCHMÄDICKE*

TECHNISCHE UNIVERSITÄT DARMSTADT, INSTITUT FÜR MINERALOGIE, SCHNITTSPAHNSTR. 9, D-64287 DARMSTADT, GERMANY

RECEIVED OCTOBER 28, 1998; REVISED TYPESCRIPT ACCEPTED JUNE 18, 1999

*Alpine-type peridotites and associated pyroxenites are found as lenses in the continental crust in many different orogens. The reconstruction of the pressure–temperature (*P–T*) evolution of these rocks is, however, difficult or even impossible. With geothermobarometry, usually one point on the overall* P–T *path can be obtained. To use the different mineral assemblages observed in ultramafic rocks as* P–T *indicators, quantitative* P–T *phase diagrams are required. This study presents new calculated phase diagrams for peridotitic and pyroxenitic rocks in the model systems CaO–MgO–Al_2O_3–SiO_2–H_2O (CMASH) and Na_2O–CaO–MgO–Al_2O_3–SiO_2–H_2O (NCMASH), which include the respective solid solutions as continuous exchange vectors. These phase diagrams represent applicable petrogenetic grids for peridotite and pyroxenite. On the basis of these general petrogenetic grids, phase diagrams for particular peridotite and pyroxenite bulk compositions are constructed. In an example of pyroxenite from the Shackleton Range, Antarctica, the different observed mineral assemblages are reflected by the phase diagrams. For these rocks, a high-pressure metamorphic stage around 18 kbar and an anticlockwise* P–T *evolution, not recognized previously, can be inferred.*

KEY WORDS: *Antarctic; high-pressure metamorphism; peridotite; phase diagrams; pyroxenite*

INTRODUCTION

Different lithologies may selectively record different stages of the same metamorphic process, hence the study of as many rock types as possible provides for a more explicit understanding of the overall metamorphic evolution of a tectonic unit. In numerous studies, metabasic eclogites have greatly been appreciated as witnesses of early high-pressure (HP) metamorphic stages, which are commonly obliterated in associated pelitic and particularly in quartzo-feldspathic rocks, especially at higher temperatures. Many of the eclogite-bearing metamorphic complexes also contain small lenses of mantle-derived peridotite and associated pyroxenite, which have not gained as much attention as pressure–temperature (*P–T*) indicators for crustal metamorphism as eclogite. However, these mantle-derived ultramafic rocks emplaced in the continental crust, although forming volumetrically minor constituents of orogenic belts, provide substantial information on the process of orogenesis and crust–mantle interaction. Thus, the study of ultramafic rocks may permit a more detailed reconstruction of the metamorphic evolution of a particular region and, in addition, these rocks may give insight into mantle processes before and/or during orogeny.

Given the existence of appropriate mineral assemblages, *P–T* data may be obtained thermobarometrically utilizing the measured compositions of mineral phases thought to be in equilibrium. In the case of peridotite and pyroxenite, with their common high-temperature imprint and their well-equilibrated high-variance mineral assemblages, this method usually results in a single *P–T* datum (e.g. Schmädicke & Evans, 1997). Depending on cooling rate, grain size, and initial temperature this reflects either the thermal peak of metamorphism or a point on the subsequent cooling path, at

*Telephone: +49-6151-163780. Fax: +49-6151-164021. e-mail: esthersc@hrzpub.tu-darmstadt.de

which the corresponding thermometer 'closed' for further diffusion.

To unravel geodynamic processes, we need to know more about the *P–T* history of metamorphic rocks than merely a single *P–T* point. An alternative strategy to obtain this information is based on the mineral assemblages and reaction textures observed in metamorphic rocks, which allow, at least, a qualitative estimation of the *P–T* path provided the relative stabilities of the mineral assemblages are known. To use this phase petrologic information in a quantitative way, complex quantitative *P–T* phase diagrams (i.e. petrogenetic grids) are needed. For a compilation of petrogenetic grids the reader is referred to Will (1998). In the case of ultramafic rocks, only very few phase diagrams are appropriate in this context, especially for medium- and high-pressure conditions. Accordingly, this study is aimed at the analysis of phase relations and the construction of quantitative *P–T* phase diagrams relevant to mantle-derived peridotites and related pyroxenites encountered in the continental crust.

PREVIOUS WORK

Examples of Alpine-type peridotite and pyroxenite, tectonically emplaced in the continental crust, are found in a number of orogens such as the Norwegian Caledonides (e.g. Carswell *et al.*, 1983; Medaris, 1984), the Eastern Alps (e.g. Morten & Obata, 1983; Obata & Morten, 1987) and Western Alps (e.g. Evans & Trommsdorff, 1978), the Dabie Mountains in China (Zhang *et al.*, 1995) or the Shackleton Range in the Antarctic (e.g. Schubert & Will, 1994). Numerous examples are known also from the European Variscides, for instance from the Schwarzwald and Vosges Mountains (Kalt *et al.*, 1995; Altherr & Kalt, 1996) and from the Bohemian Massif, where mantle-derived ultramafics occur in different tectonic units [for reviews, see Medaris & Carswell (1990) and Schmädicke & Evans (1997)]. The dominant mineral phases in these peridotites are olivine, orthopyroxene, clinopyroxene, garnet and/or spinel, chlorite, and calcic amphibole. In some cases, peridotite contains interlayers or boudins of pyroxenite, mainly consisting of clinopyroxene and orthopyroxene, with or without garnet, spinel, plagioclase, calcic amphibole, chlorite, olivine, and quartz.

The common high-pressure assemblages in these rocks are garnet–orthopyroxene–clinopyroxene–olivine (peridotite) or garnet–orthopyroxene–clinopyroxene (pyroxenite). These, generally well-equilibrated assemblages, allow the application of the garnet–orthopyroxene (e.g. Harley, 1984*b*), garnet–clinopyroxene (e.g. Powell, 1985), or garnet–olivine (e.g. Brey & Köhler, 1990) $Mg_{-1}Fe$ exchange thermometers, as well as the two-pyroxene solvus thermometer (e.g. Brey & Köhler, 1990). Pressure can be confined by the 'Al-in-orthopyroxene' (e.g. Harley, 1984*a*) or the 'Cr-in-spinel' (e.g. O'Neill, 1981) barometers. These thermobarometers combined yield usually one *P–T* datum. Additionally occurring chlorite and calcic amphibole are often interpreted as 'secondary phases' and not much attention is paid to them. Undeniably, the equilibration conditions of these phases are almost impossible to assess, as no adequate thermobarometer is available and/or the phase relations and equilibrium assemblages of retrograde metamorphic stages are hard to define, mainly because equilibration is incomplete.

Complex phase diagrams containing all the major and minor phases important in peridotite and pyroxenite and giving the stabilities of the different assemblages may help to define the *P–T* conditions and, in particular, the *P–T* evolution more closely. However, there is only a small number of phase diagrams available so far, which apply to medium- and high-pressure ultramafic rocks. Qualitative petrogenetic grids were constructed by Medaris & Carswell (1990) and Obata & Thompson (1981) on the basis of mineral assemblages observed in peridotites, combined with theoretical phase petrologic considerations. These diagrams reveal that the aluminous phases garnet, spinel, plagioclase, calcic amphibole, and chlorite are the important ones indicative of *P* and *T*.

Quantitative phase diagrams containing the phases relevant for peridotite and pyroxenite are not available so far, with the exception of the petrogenetic grid of Jenkins (1981) for peridotite in the model system CaO–MgO–Al_2O_3–SiO_2–H_2O (CMASH). This diagram (Fig. 1) represents the most complex quantitative approach to the phase relations of medium- and high-pressure peridotitic rocks hitherto. It is based on the experimentally determined positions of several important reactions. Judging from the experimental data, additional reaction curves in Fig. 1 are semi-quantitatively derived by phase petrologic constraints. According to this diagram, chlorite and calcic amphibole are stable in peridotites at temperatures not exceeding 850°C. The stability of calcic amphibole, with forsterite in excess, is confined to pressures below about 14 kbar whereas chlorite can be stable to much higher pressures. Garnet is not formed below 16 kbar and, therefore, according to this phase diagram a coexistence of garnet and calcic amphibole is precluded in peridotite.

This, however, is in contrast to the phase relations observed in natural peridotite. Garnet and calcic amphibole are known to coexist in peridotites, for instance, in those from the Erzgebirge Crystalline Complex (Schmädicke & Evans, 1997) or those from the Granulitgebirge in southeastern Germany (Fig. 2). Consequently, the application of the petrogenetic grid of Jenkins (1981) for the quantitative reconstruction of the

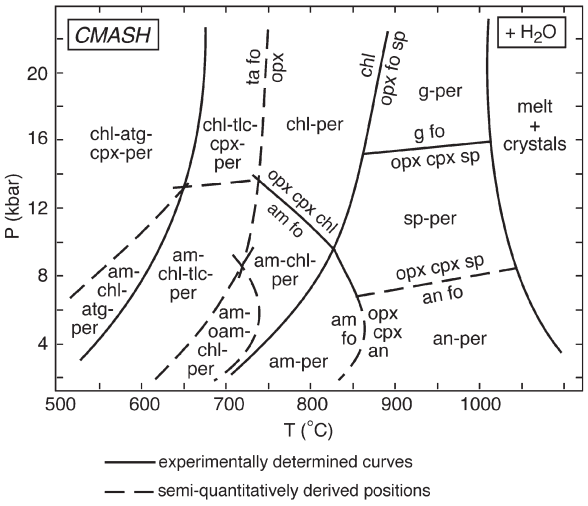

Fig. 1. Petrogenetic grid for peridotitic rocks in the model system $CaO–MgO–Al_2O_3–SiO_2–H_2O$ after Jenkins (1981). atg, antigorite; oam, orthoamphibole; ta, Mg-end-member talc; tlc, Mg-talc with Tschermak's substitution; per, peridotite. Other abbreviations as given in Table 1.

P–T evolution of peridotites is limited. New, quantitative phase diagrams are needed to use the entire phase information available from peridotite and pyroxenite in a quantitative way.

PHASE DIAGRAM CALCULATIONS

The possibility to obtain information on mineral reactions and stability relations of mineral assemblages is given by thermodynamic calculations, using internally consistent thermodynamic data. With this method, theoretical phase diagrams can be constructed. Because, in nature, the compositions of solid solution phases change with *P* and *T*, it is important to account for these compositional changes in the phase diagram. This is possible with the computer program THERMOCALC (Powell & Holland, 1988), which is used here together with the thermodynamic dataset (September 1993 version) of Holland & Powell (1990). Solid solutions are treated as continuous exchange vectors, and the calculated phase diagrams should be a closer approximation to reality than the commonly used diagrams with minerals at end-member or fixed compositions.

In addition, with the capability to model changing compositions, it also is possible to construct phase diagrams for particular bulk-rock chemistries, showing not only the stabilities of univariant reactions but also of di- or trivariant assemblages relevant to individual rocks. These diagrams, also known as 'pseudosections' (Hensen, 1971; Will *et al.*, 1990) provide a very helpful tool for extracting *P–T* information or *P–T* path information, simply from the assemblages or sequences of assemblages observed in thin sections. Moreover, the modelled compositions of solid solutions in a particular assemblage, compared with the compositions of minerals in natural parageneses, give further clues to metamorphic *P–T* conditions. Utilizing this method, new phase diagrams for ultramafic rocks can be calculated and constructed. [For more details on the method, see Powell *et al.* (1998).]

CMASH system

To study the phase relations of ultramafic rocks, the model system $CaO–MgO–Al_2O_3–SiO_2–H_2O$ (CMASH) was chosen, with water in excess. This provides an opportunity to compare the modelled equilibria with the petrogenetic grid of Jenkins (1981). The considered phases are listed in Table 1. There are only four end-member phases, spinel, forsterite, anorthite and quartz. The last was included to apply the phase diagrams, at least to some extent, to metabasic rocks. In the CMASH model system, two types of solid solutions occur: the Tschermak's substitution, $Mg_{-1}Si_{-1}AlAl$, in orthopyroxene, clinopyroxene, calcic amphibole and chlorite, and the $Mg_{-1}Ca$ exchange in garnet. Ideal molecular solution models were chosen to describe these substitutions, after various models had been tested (see below).

The calculated phase diagram is depicted in Fig. 3, and the corresponding invariant *P–T–X* data are compiled in Table 2. As the diagram includes all stable reactions possible among the involved phases, it is, inevitably, rather complex. Naturally, not all these reactions occur in a single rock. A particular rock will only 'see' parts of the reactions in Fig. 3, depending upon its bulk-rock composition. On the basis of the *P–T* diagram in Fig. 3, specific diagrams can be constructed for any given bulk-rock chemistry. This is possible as THERMOCALC computes the compositions of solid solution phases in any assemblage for any *P* and *T*. The advantage thereby is that not only the univariant reactions relevant to a particular rock can be identified but also the di- or trivariant assemblages that are stable between the reactions (see below).

CMASH diagram for peridotite

A quantitative phase diagram calculated from Fig. 3 for a specific peridotite composition is shown in Fig. 4. With other peridotite compositions, there is little or no change in the topology with respect to Fig. 4, only the modal phase proportions change to some extent with bulk compositional changes. This is visualized in the $SiO_2–Al_2O_3–MgO$ compatibility diagrams (Fig. 5). Thus, in this case, the phase diagram topology is not very sensitive to compositional changes, as long as the composition is

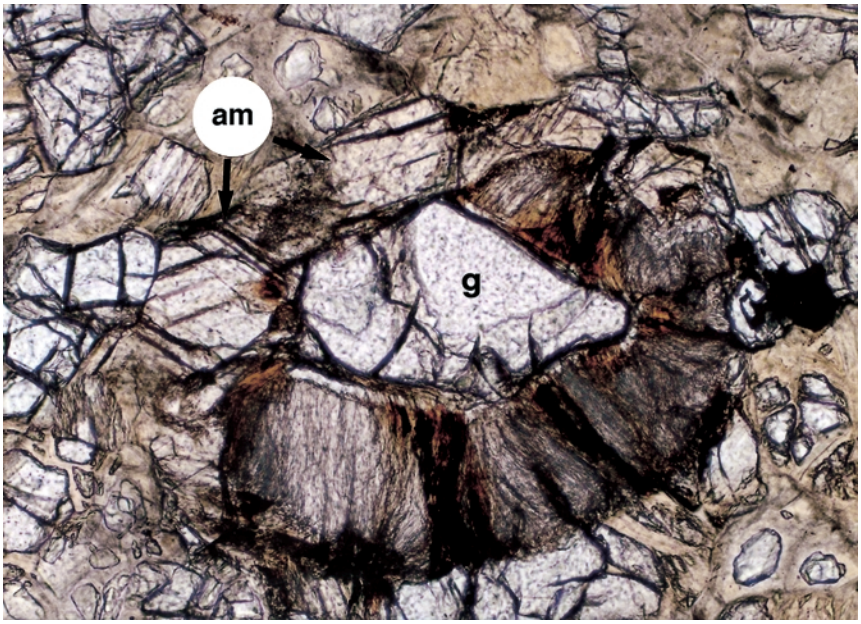

Fig. 2. Photomicrograph of a garnet peridotite from the Granulitgebirge, Bohemian Massif (sample Rub95-1). In this partly serpentinized rock, calcic amphibole coexists with the garnet–olivine–orthopyroxene–clinopyroxene assemblage. Garnet (g) is partially replaced by a rim of spinel-bearing symplectite and shares straight grain boundaries with calcic amphibole (am). This intergrowth texture testifies that calcic amphibole was formed in the garnet peridotite stability field, before partial transformation to spinel peridotite occurred. Plane-polarized light; horizontal field of view 3·3 mm.

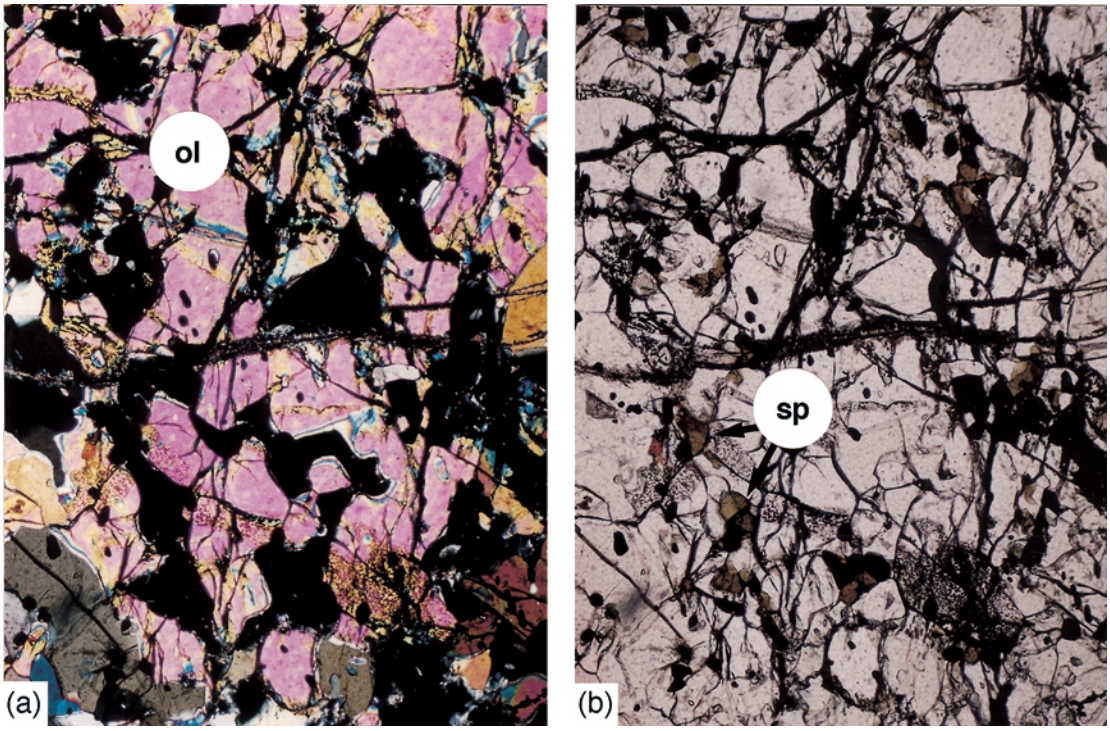

Fig. 10. Photomicrograph of garnet pyroxenite W216 from the Shackleton Range, Antarctica. Intergrowths of garnet and olivine (ol) are ascribed to the reaction opx + cpx + sp → g + fo. Small 'left-over' grains of greenish brown spinel (sp), preferably included in garnet, additionally point to this reaction. (a) Crossed polars, (b) plane-polarized light; vertical field of view 2·5 mm.

Table 1: Phases and phase components considered in Fig. 3 (CMASH) and Fig. 8 (NCMASH)

Phases	Phase components	
CMASH		
garnet (g)	pyrope (py)	$Mg_3Al_2[Si_3O_{12}]$
	grossular (grs)	$Ca_3Al_2[Si_3O_{12}]$
orthopyroxene (opx)	enstatite (en)	$MgMg[Si_2O_6]$
	Mg-Tschermak's (mgts)	$MgAl[AlSiO_6]$
clinopyroxene (cpx)	diopside (di)	$CaMg[Si_2O_6]$
	Ca-Tschermak's (cats)	$CaAl[AlSiO_6]$
calcic amphibole (am)	tremolite (tr)	$Ca_2Mg_3Mg_2[Si_4Si_4O_{22}](OH_2)$
	tschermakite (ts)	$Ca_2Mg_3Al_2[Si_4Al_2Si_2O_{22}](OH_2)$
chlorite (chl)	clinochlore (clin)	$Mg_4MgAl[Si_2AlSiO_{10}](OH)_8$
	amesite (ames)	$Mg_4Al_2[Si_2Al_2O_{10}](OH)_8$
spinel (sp)		$MgAl_2O_4$
forsterite (fo)		$Mg_2[SiO_4]$
anorthite (an)		$Ca[Al_2Si_2O_8]$
quartz (q)		SiO_2
NCMASH		
garnet (g)	see CMASH	
orthopyroxene (opx)	see CMASH	
clinopyroxene (cpx)	diopside (di)	$CaMg[Si_2O_6]$
	Ca-Tschermak's (cats)	$CaAl[AlSiO_6]$
	jadeite (jd)	$NaAl[Si_2O_6]$
calcic amphibole (am)	tremolite (tr)	$Ca_2Mg_3Mg_2[Si_4Si_4O_{22}](OH_2)$
	pargasite (prg)	$NaCa_2Mg_3MgAl[Si_4Al_2Si_2O_{22}](OH_2)$
chlorite (chl)	see CMASH	
spinel (sp)	see CMASH	
forsterite (fo)	see CMASH	
plagioclase (pl)	anorthite (an)	$Ca[Al_2Si_2O_8]$
	albite (ab)	$Na[AlSi_3O_8]$

peridotitic, and the topology shown in Fig. 4 is representative for the phase relations in peridotites in the CMASH model system. The diagram in Fig. 4 is far less complex than that in Fig. 3, and contains only four of the 13 stable invariant points of Fig. 3. The assemblages stable between the univariant reactions are all divariant.

The stabilities of the assemblages in the calculated CMASH phase diagram (Fig. 4) closely match those in Jenkins' (1981) diagram (Fig. 1). In addition, the calculated reaction positions correspond very well to experimental data. The calculated garnet–spinel peridotite transition reaction g + fo = opx + cpx + sp even changes to a negative slope at low temperatures (this metastable part is not shown in Figs 3 and 4), in coincidence with experimental results (e.g. Danckwerth & Newton, 1978; Gasparik, 1987). Furthermore, the computed Al content in orthopyroxene in the divariant field g–opx–cpx–fo (Fig. 4) is in close agreement with experimental data (e.g. Harley, 1984*a*). These solid solution compositions can be used as further *P–T* constraints in the relatively large divariant fields. In the divariant assemblage g–opx–cpx–fo, the Al content of opx is strongly P sensitive; in fact, this relation was calibrated as a barometer by several workers (e.g. Harley, 1984*a*; Brey *et al.*, 1986). In contrast, in the divariant assemblages chl–opx–cpx–fo, chl–opx–am–fo and sp–opx–cpx–fo, the Al-content in opx is an indicator of temperature rather than pressure.

Furthermore, the modelled compositions of solid solutions (e.g. see Table 2 for invariant points) compare well with those found in natural peridotites (e.g. Schmädicke & Evans, 1997). For instance, garnet in peridotite is pyrope

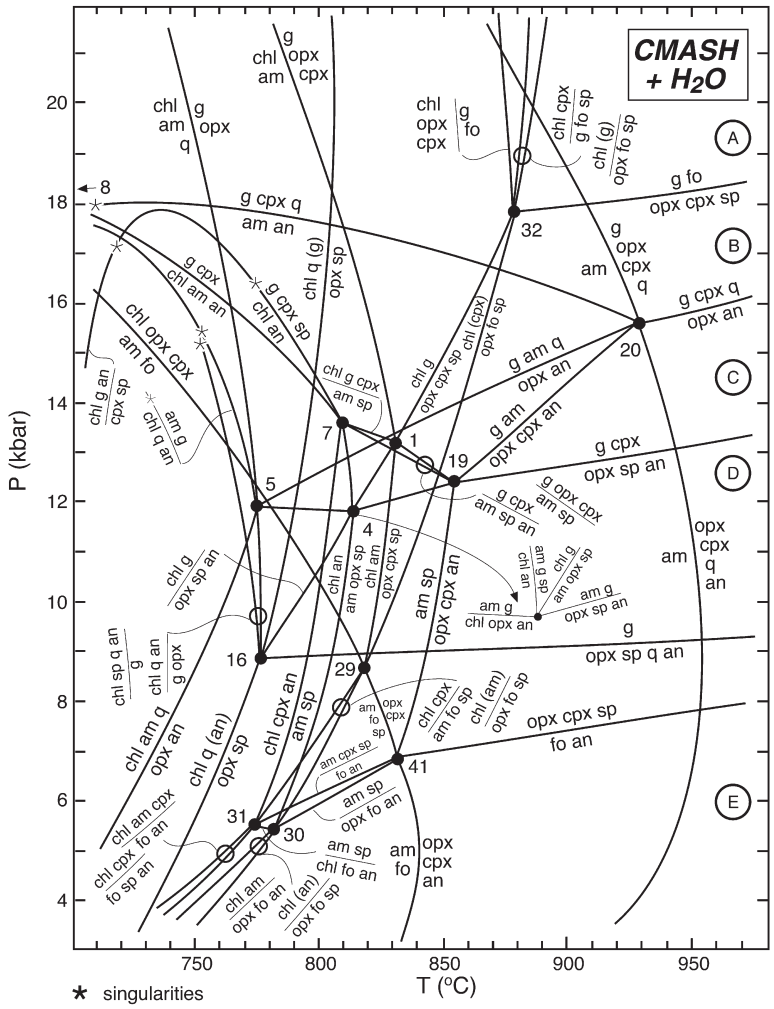

Fig. 3. *P–T* phase diagram for ultramafic (and mafic) rocks in the model system CaO–MgO–Al_2O_3–SiO_2–H_2O (water in excess). The Tschermak's substitution, $Mg_{-1}Si_{-1}AlAl$, in orthopyroxene, clinopyroxene, calcic amphibole and chlorite, and the $Mg_{-1}Ca$ substitution in garnet are treated as continuous exchange vectors and are described by ideal molecular solution models. Thus, the compositions of the solid solution phases change along the univariant reactions and over di- and trivariant fields. For the mineral compositions at invariant points, the reader is referred to Table 2. The compatibility diagrams for fields A–E are shown in Fig. 5.

rich, with a grossular component around 5 mol %. The only 'garnet-bearing' invariant point (32) in Fig. 4 involves garnet with 5 mol % grossular. This composition does not change much along the univariant curves and within the divariant field (see isopleths in Fig. 4), again in agreement with garnet compositions in natural peridotite. In addition, the calculated amount of Tschermak's component in the pyroxenes agrees well with compositions known from natural assemblages: clinopyroxene invariably contains more Tschermak's component than coexisting orthopyroxene (see Table 2, Fig. 4).

As the calculated equilibria are in good agreement with available experimental results, and the calculated solid solution compositions are similar to natural ones, the applied molecular mixing models seem to be reasonable in this context. In contrast, this is not the case with ionic solution models, both ideal and non-ideal. For instance, the garnet–spinel peridotite transition reaction shifts to a pressure of 8–9 kbar, being in indisputable disagreement with experimental data and petrologic constraints. In addition, with ionic mixing models, the modelled compositions of solid solutions do not correspond to natural mineral compositions. Along the spinel–garnet peridotite transition reaction, for instance, garnet contains around 30 mol % grossular, about six times as much as in nature and with molecular models.

In conclusion, with ideal molecular mixing models not only the experimentally determined reaction positions can be reproduced, but also the compositions of natural solid solutions. However, in the petrogenetic grid for

Table 2: P–T–X positions of stable invariant CMASH points as seen in Fig. 3 (H_2O in excess)

Point	*P* (kbar)	*T* (°C)	X_{grs}(g)	X_{cats}(cpx)	X_{mgts}(opx)	X_{ames}(chl)	X_{ts}(am)
1: [fo,q,an]	13·2	831	0·05	0·18	0·14	0·18	0·27
	13·6	*725*	*0·07*	*0·13*	*0·10*	*0·17*	*0·23*
4: [cpx,fo,q]	11·8	814	0·03		0·16	0·22	0·30
	10·8	*699*	*0·02*		*0·14*	*0·25*	*0·28*
5: [cpx,fo,sp]	11·9	773	0·01		0·15	0·22	0·29
	10·9	*678*	*0·01*		*0·13*	*0·25*	*0·28*
7: [opx,fo,q]	13·6	808	0·09		0·24	0·26	0·32
	14·0	*685*	*0·20*		*0·25*	*0·32*	*0·33*
8: [opx,fo,sp]	17·9	692	0·56	0·29		0·34	0·35
	—	—					
29: [g,q,an]	8·7	818		0·12	0·09	0·14	0·22
	9·5	*720*		*0·09*	*0·07*	*0·13*	*0·18*
30: [g,cpx,q]	5·4	780			0·08	0·14	0·21
	3·6	*666*			*0·06*	*0·15*	*0·17*
31: [g,opx,q]	5·5	774		0·11		0·14	0·21
	3·8	*657*		*0·08*		*0·15*	*0·17*
32: [am,q,an]	17·8	877	0·05	0·12	0·10	0·10	
	17·5	*753*	*0·06*	*0·09*	*0·07*	*0·10*	
16: [am,cpx,fo]	8·9	776	0·00		0·22	0·34	
	8·9	*681*	*0·00*		*0·18*	*0·33*	
19: [chl,fo,q]	12·4	854	0·05	0·20	0·16		0·30
	11·9	*771*	*0·06*	*0·18*	*0·14*		*0·28*
20: [chl,fo,sp]	15·6	928	0·05	0·17	0·13		0·27
	14·5	*826*	*0·05*	*0·15*	*0·12*		*0·25*
41: [chl,g,q]	7·0	831		0·12	0·09		0·22
	6·3	*750*		*0·10*	*0·07*		*0·20*

Data for a_{H_2O} = 0·5 (italics) are given for comparison. Phases not present at the respective invariant point appear in square brackets. Abbreviations of phases and phase components are given in Table 1. X_{grs}(g) is mole fraction of grossular in garnet; $X_{grs}(g) + X_{py}(g) = 1$.

peridotites (Fig. 4) calculated in this study, there still is the same problem as in Jenkins' (1981) phase diagram: garnet and calcic amphibole cannot coexist. This, however, contradicts the behaviour in nature (see above). Having approved of the mixing models, the most probable explanation for this discrepancy is that the CMASH model system is obviously not the best choice to portray the phase relations of peridotites, at least, as far as the stability of calcic amphibole is concerned. One or more further system component(s) must be crucial in this respect. Indeed, the calcic amphibole found in peridotite to coexist with garnet is a pargasite or pargasitic hornblende (e.g. Schmädicke & Evans, 1997). Sodium is, therefore, an important component for the stabilization of calcic amphibole in peridotite, as emphasized also by Obata & Thompson (1981). Thus, to portray the phase relations of peridotites, the phase diagram calculations are expanded to the NCMASH model system (see below).

CMASH diagrams for pyroxenite

From Fig. 3, *P–T* phase diagrams for different pyroxenitic bulk-rock compositions were calculated (Figs 6 and 7) in the same way as was done for peridotite (Fig. 4). In contrast to peridotitic bulk compositions, which may vary to some extent without changing the topology of Fig. 4, phase diagrams for pyroxenitic rocks are far more sensitive to bulk chemical variations. This becomes obvious in the compatibility diagrams (Fig. 5) displaying the assemblages stable in different *P–T* fields as a function of bulk-rock composition. In field A, for instance, only one divariant assemblage is 'seen' in peridotites whereas five divariant assemblages are possible in the compositional range of pyroxenites.

The pyroxenite in Fig. 6 (analysis of a sample from the Granulitgebirge) will see only three out of the 13 invariant points in Fig. 3. The pyroxenite in Fig. 7 (analysis from an Erzgebirge sample) contains more

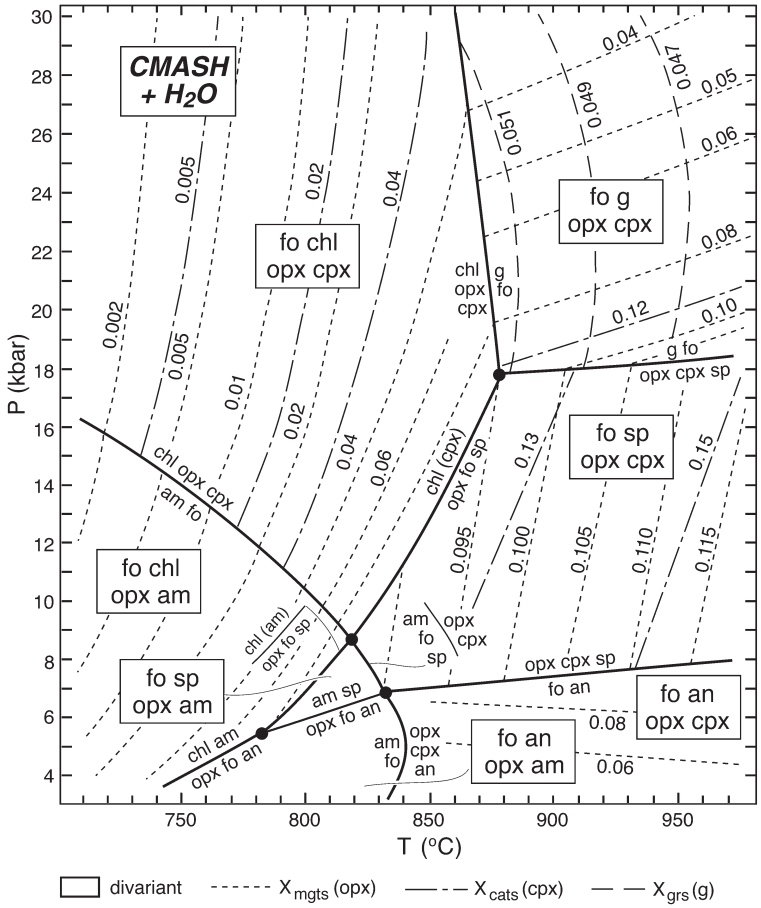

Fig. 4. *P–T* phase diagram constructed from Fig. 3, displaying the univariant reactions and stabilities of divariant assemblages 'seen' by a peridotite. The diagram was calculated for the composition (in wt %) CaO = 2·2, MgO (+FeO) = 39·9, Al_2O_3 = 3·0, SiO_2 = 38·8. With other peridotite compositions, however, there is little or no change in the phase diagram topology (see also Fig. 5). The divariant fields are contoured for X_{grs} in garnet and X_{mgts} in orthopyroxene; a few isopleths for X_{cats} in clinopyroxene are given for comparison.

MgO (+FeO) and less CaO than the rock in Fig. 6. This composition yields a markedly different topology, with eight stable invariant points. In the upper right corners of the *P–T* pseudosections, at highest *P* and *T* (field A), the pyroxenite from the Granulitgebirge is composed of the trivariant assemblage g–opx–cpx, whereas the pyroxenite from the Erzgebirge is characterized by a divariant paragenesis of g–q–opx–cpx (see also Fig. 5). This example highlights the importance of constructing *P–T* diagrams for specific bulk-rock compositions, if the stability of a mineral assemblage is to be assessed. Having established the successive sequences of mineral assemblages in a rock from petrographic observations, these pseudosections are of valuable help to 'translate' the petrographic data into the *P* and *T* experienced by a rock through its metamorphic history. This will be further demonstrated with the example of pyroxenite from the Shackleton Range, Antarctica (see below).

NCMASH system

The phase diagram in the model system Na_2O–CaO–MgO–Al_2O_3–SiO_2–H_2O (NCMASH) is shown in Fig. 8. As this diagram was particularly constructed for peridotite, quartz is not considered here. The new system component Na_2O enters three phases: calcic amphibole, plagioclase and clinopyroxene. The respective phase components are listed in Table 1. Again, ideal molecular mixing models were used. The NCMASH phase diagram is less complex than the CMASH grid (Fig. 3), and has only three stable invariant NCMASH points in the *P–T* window considered (Fig. 8, Table 3). In part, this is due to the fact that quartz is omitted from the NCMASH diagram. Therefore, only the nine invariant points and emanating reactions in Fig. 3 without quartz can be compared with Fig. 8. It is obvious that, according to the phase rule, the invariant points in CMASH turn to univariant reactions in NCMASH. To illustrate this relationship, some of the CMASH invariant points are

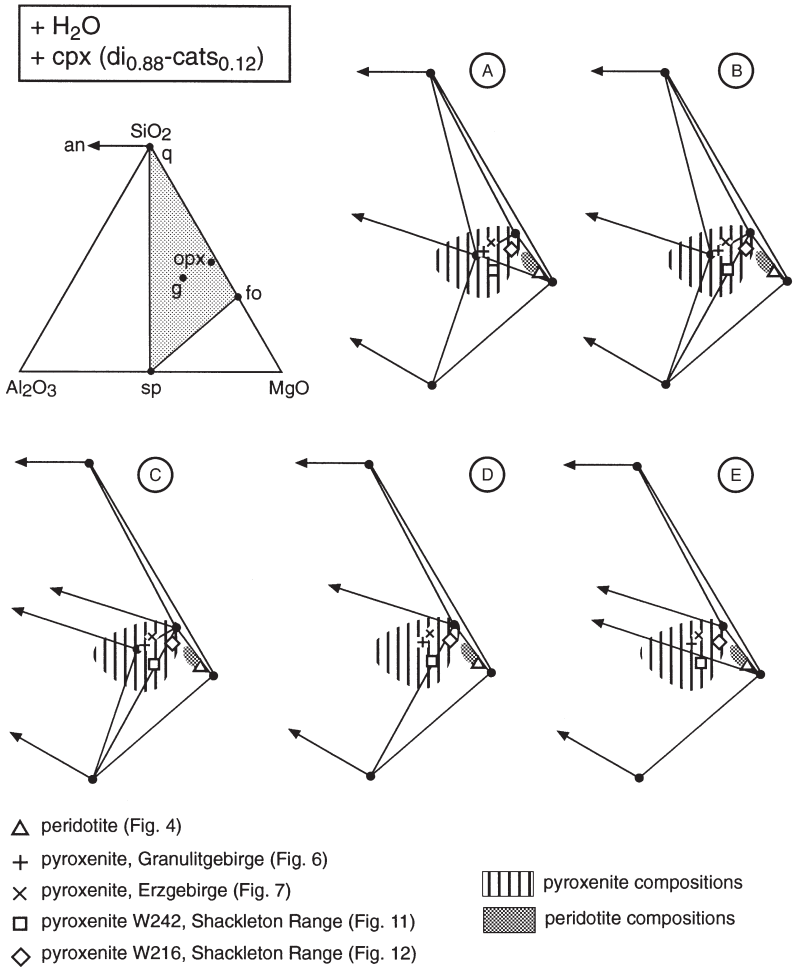

Fig. 5. Compatibility diagrams, projected from water and clinopyroxene, for the *P–T* fields indicated in Fig. 3. The compositional range of clinopyroxene-bearing peridotitic and pyroxenitic rocks [analyses from Nixon (1987) and Wilson (1989)] is illustrated along with the bulk-rock compositions used for the construction of specific *P–T* diagrams (Figs 4, 6, 7, 11 and 12). For instance, in field A, only the divariant assemblage g–fo–opx–cpx is 'seen' in peridotites whereas five divariant assemblages are possible in pyroxenites: g–fo–opx–cpx, g–fo–sp–cpx, g–sp–an–cpx, g–an–q–cpx, and g–opx–q–cpx. It should be noted that in nature in Al_2O_3-rich rocks, anorthite may be metastable at high pressure (fields A and B) with respect to kyanite-bearing assemblages. However, this applies only to pyroxenite compositions plotting on the left-hand side of the line sp–g–q.

added to Fig. 8. Using exactly the same bulk-rock composition as in Fig. 4, with only a small additional amount of Na_2O, a specific *P–T* diagram for a peridotite was obtained (Fig. 9).

In Fig. 9, the transition reactions from plagioclase to spinel to garnet peridotite take place at basically the same *P–T* conditions as in the CMASH system. This is because either little Na enters the respective solid solution phases or the reaction coefficients of the Na-bearing phases are small. In contrast to Fig. 4, calcic amphibole is now stable to much higher pressures, and can coexist with garnet in a divariant field from about 18 to 26 kbar pressure. At higher pressures, a peridotite will contain the well-known four-phase garnet peridotite assemblage g–opx–cpx–fo, which is trivariant in NCMASH. The breakdown of amphibole with increasing pressure takes place via a 'divariant reaction'. This means that the modal proportion of amphibole steadily decreases with increasing pressure until it approaches zero and amphibole disappears (see contours of amphibole content in Fig. 9). The pressure at which amphibole reacts out depends on the bulk Na content of the rock; thus, in peridotites with a composition different from that in Fig. 9 amphibole will disappear at somewhat lower or higher pressure. It should be noted that the calculated pressure stability of calcic amphibole in this system corresponds well to that of amphibole in natural metabasite, as experimentally constrained by Pawley & Holloway (1993).

Comparing the calculated compositions of the Na-bearing phases (Table 3, and isopleths in Fig. 9) with

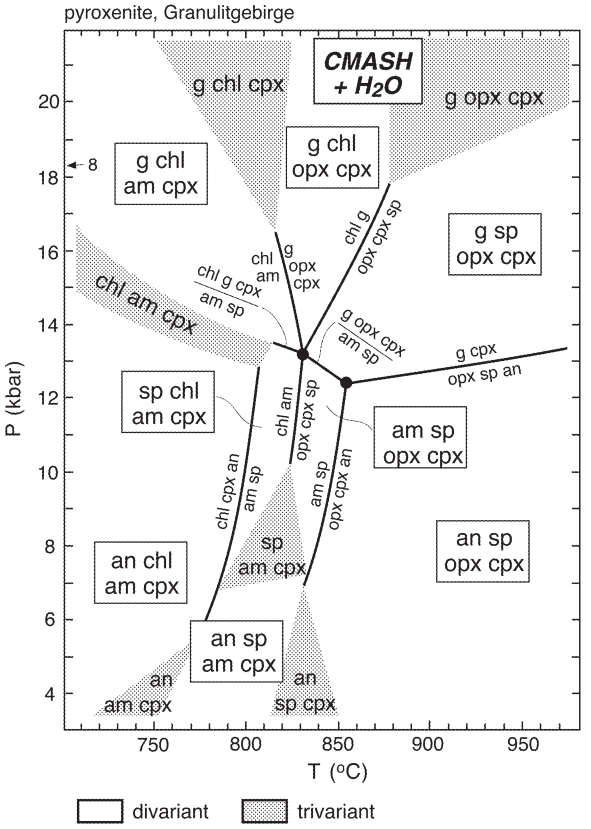

Fig. 6. *P–T* diagram for a pyroxenitic rock with the bulk composition (in wt %) CaO = 14·1, MgO (+FeO) = 23·5, Al_2O_3 = 13·2, SiO_2 = 45·3 (analysis of a rock from the Granulitgebirge, Bohemian Massif), constructed from the complex phase diagram in Fig. 3.

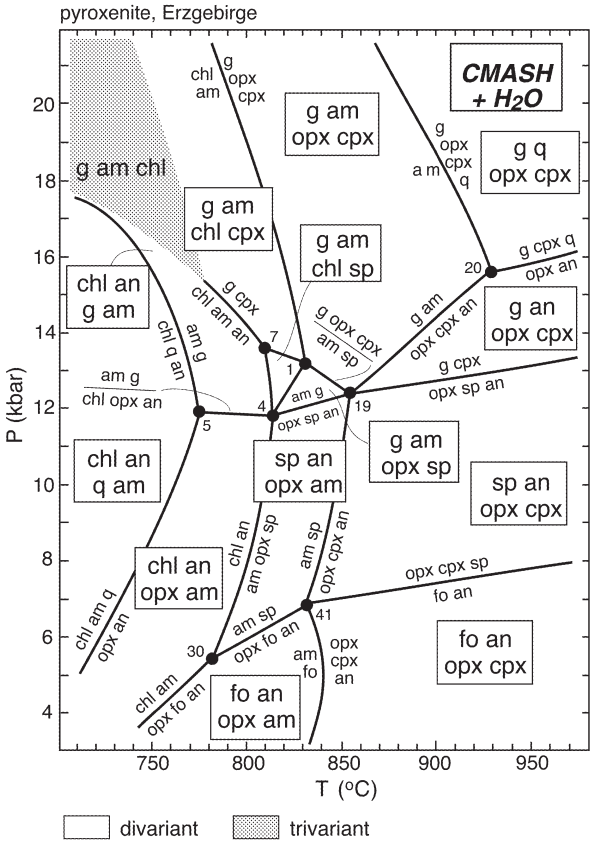

Fig. 7. Petrogenetic grid for a pyroxenitic rock with the bulk-rock composition (in wt %) CaO = 9·0, MgO (+FeO) = 26·4, Al_2O_3 = 14·3, SiO_2 = 46·6 (analysis of a rock from the Erzgebirge, Bohemian Massif) constructed from Fig. 3. It should be noted that this rock differs from the pyroxenite in Fig. 6 in the CaO and the MgO (+FeO) content, causing a different phase diagram topology.

natural minerals, there is a good coincidence between the two. For instance, in peridotitic rocks, the amphibole which coexists with garnet is invariably Na rich, whereas amphibole in low-pressure assemblages with chlorite is more tremolitic (e.g. Schmädicke & Evans, 1997).

APPLICATION OF THE CMASH SYSTEM TO PYROXENITE FROM THE SHACKLETON RANGE, ANTARCTICA

Geological setting and investigated samples

The Shackleton Range is part of the Cambro-Ordovician Ross orogen in the Antarctic, extending from northern Victoria Land through the Transantarctic and Pensacola Mountains to the Shackleton Range. In contrast to the general N–S trend in the main part of the Ross orogen, in the Shackleton Range, the structural trend changes to E–W (e.g. Kleinschmidt & Buggisch, 1994). The Shackleton Range Metamorphic Complex consisting of medium- to high-grade metamorphic rocks can be divided into (1) the 'Read Mountains Basement Complex' in the south and (2) the 'Northern Shackleton Range Basement Complex' (e.g. Buggisch *et al.*, 1990; Kleinschmidt & Buggisch, 1994). These crystalline complexes differ in both their metamorphic record and plate tectonic position. The Read Mountains Basement Complex represents Precambrian basement of the East Antarctic Craton, whereas the Northern Shackleton Range Basement Complex was strongly affected by deformation and metamorphism during the Ross orogeny (480–500 Ma; e.g. Kleinschmidt & Buggisch, 1994). That orogeny was also responsible for southward thrusting of the Northern Crystalline Complex and back-arc basin sediments over the Read Mountains Complex (Buggisch *et al.*, 1990). As the transition between the East Antarctic Craton and the Ross orogen is exposed in the Shackleton Range, this area is of special importance for geotectonic reconstructions.

Ultramafic rocks, predominantly pyroxenites, were found around Mount Provender within the Haskard

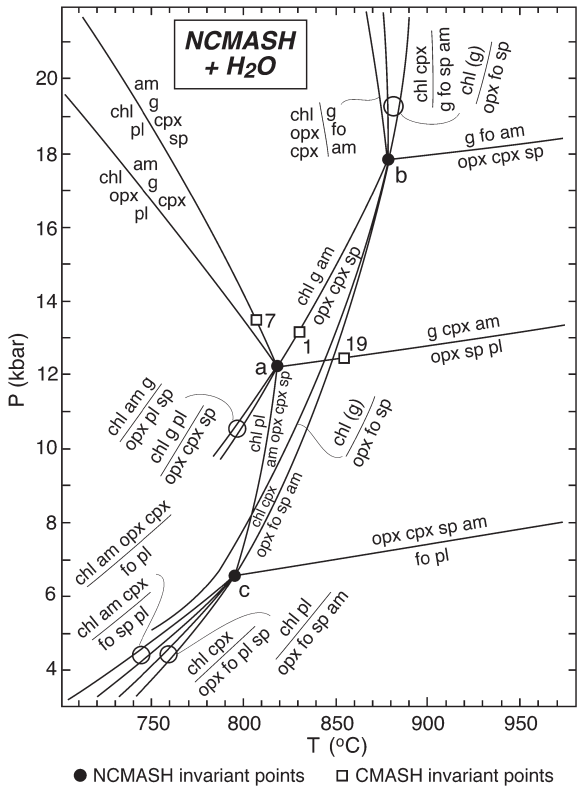

Fig. 8. Calculated phase diagram for ultramafic rocks in the model system Na_2O–CaO–MgO–Al_2O_3–SiO_2–H_2O (water in excess). All solid solutions (see Table 1) are described by ideal molecular models. The *P–T–X* data for the invariant points are given in Table 3.

Highlands, situated in the northwestern part of the Northern Shackleton Range Basement Complex (Grew & Halpern, 1979; Schubert & Will, 1994; Marx, 1996). Apart from ultramafic rocks, the Mount Provender area includes migmatitic hornblende-bearing gneiss, marble, calc-silicate rocks, kyanite schist, quartzite, granulite, amphibolite, and garnetiferous gneiss (Grew & Halpern, 1979). Mineral assemblages testify to metamorphic conditions in the upper amphibolite and granulite facies. Ultramafic rocks occur as lenses with a size ranging from a few metres up to about 100 m (W. Schubert, personal communication, 1998).

Samples from two different lenses of pyroxenite, W216 and W242, about 1 km apart, are considered here. The host rocks are: garnet–kyanite gneiss, clinopyroxene-bearing gneiss and calc-silicate rocks (W216) and garnet amphibolite and garnet quartzite (W242) (Schubert & Will, 1994; Marx, 1996). The pyroxenite samples may show a weak foliation, mainly defined by calcic amphibole, orthopyroxene and/or olivine and, in some cases, even by garnet. Pyroxenite W242 is characterized by different equilibrium domains. The prominent mineral assemblage garnet–green spinel–orthopyroxene–clinopyroxene is ascribed to a second equilibration stage (II). An earlier garnet-free assemblage (I) can be inferred texturally. Later, retrograde assemblages are dominated by calcic amphibole, whereas in some domains garnet can be observed to coexist with calcic amphibole and chlorite (III), and in other domains garnet is absent and anorthite (IV) occurs. Spinel is not present in either of these later assemblages. In sample W216 two succeeding parageneses are texturally indicated: olivine–brownish green spinel–orthopyroxene–clinopyroxene (I), and olivine–garnet–orthopyroxene–clinopyroxene (II) (Fig. 10). Furthermore, calcic amphibole can be observed, which probably belongs to a later assemblage.

Phase diagrams and *P–T* path reconstruction

On the basis of bulk-rock analyses of small samples, representing the thin-section scale (see figure captions), specific phase diagrams were calculated for each sample (Figs 11 and 12). For sample W242 (Fig. 11), a relatively small divariant field confines the stability of assemblage II at a pressure between 16 and 18 kbar. Assemblages III and IV correspond to the partial retrograde equilibration stages indicated in the respective fields in Fig. 11.

The *P–T* evolution of granulitic host rocks, reconstructed by Schubert & Will (1994), is depicted in Fig. 11. Two succeeding equilibration stages of 660°C and 13·5 kbar, and 740°C and 9 kbar define a clockwise *P–T* trend. Assuming that the *P–T* trajectories of pyroxenite and granulite converge at some stage and considering the stability fields of the retrograde equilibration stages in the phase diagram, a *P–T* path for the pyroxenite as shown in Fig. 11 can be derived. So far, it is not clear whether the *P–T* segment from II to IV is part of a clockwise or an anticlockwise *P–T* evolution. Stage I may be attributed to similar or lower pressures than II, allowing both possibilities.

The transition from stage I to II in sample W216 (Fig. 12) is essentially induced by an increase in pressure. Inclusions of spinel in garnet and the intergrowth of garnet with olivine, in places resembling coarse symplectites (Fig. 10), are ascribed to the nearly isobaric reaction opx + cpx + sp → g + fo (transition from field I to field II in Fig. 10). From pyroxenite W216 alone, the evolution of temperature during this compressional stage is difficult to assess.

The *P–T* information for the two samples, W242 and W216, combined, points to an overall *P–T* evolution involving early compression and cooling before decompression and further cooling, and suggests an anticlockwise *P–T* trajectory rather than a clockwise evolution. The peak pressure conditions experienced by the pyroxenite are close to the CMASH univariant reaction opx + cpx + sp = g + fo (~18 kbar), which,

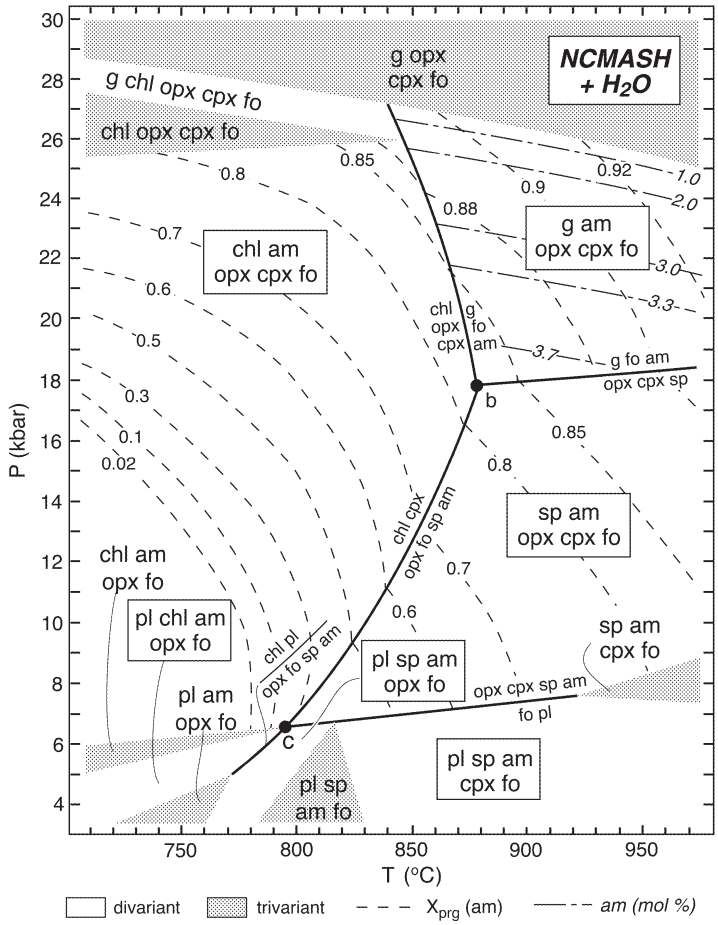

Fig. 9. *P–T* phase diagram as in Fig. 8, displaying the univariant reactions and stabilities of di- and trivariant assemblages 'seen' by a peridotite [composition (in wt %) $Na_2O = 0{\cdot}13$, $CaO = 2{\cdot}2$, $MgO\ (+FeO) = 39{\cdot}9$, $Al_2O_3 = 3{\cdot}0$, $SiO_2 = 38{\cdot}8$]. It should be noted that the composition, with the exception of additional Na_2O, is the same as in Fig. 4.

Table 3: P–T–X positions of stable invariant NCMASH points as seen in Fig. 8 (H_2O in excess)

Point	*P* (kbar)	*T* (°C)	X_{grs}(g)	X_{cats}(cpx)	X_{mgts}(opx)	X_{ames}(chl)	X_{jd}(cpx)	X_{prg}(am)	X_{ab}(pl)
a: [fo,q]	12·2	818	0·054	0·19	0·15	0·21	0·003	0·44	0·01
b: [pl,q]	17·8	873	0·051	0·12	0·09	0·11	0·005	0·82	
c: [g,q]	6·7	796		0·11	0·08	0·14	0·000	0·23	0·003

Labelling is as in Table 2; abbreviations are explained in Table 1.

in case of sample W216, was overstepped whereas the phase relations in sample W242 point to a pressure closely below this reaction. Using mineral compositional data (Marx, 1996), the maximum pressure of sample W216 can independently be constrained: the 'Al-in-opx-barometer' (Harley, 1984*a*; Brey *et al.*, 1986) and the 'Cr-in-sp-barometer' (O'Neill, 1981) yield a pressure of 17–18 kbar and 18–19 kbar at $T = 800$°C and about half a kilobar more at $T = 900$°C, respectively, indicating that the peak pressure conditions of the two studied samples are indeed very similar, as expected because they belong to the same tectonic unit. The same pressure can be estimated utilizing the isopleths for the Mg-Tschermak's component in orthopyroxene in Fig. 4. Temperature estimates on garnet–olivine pairs in sample W216 range between 870 and 910°C applying the ap-

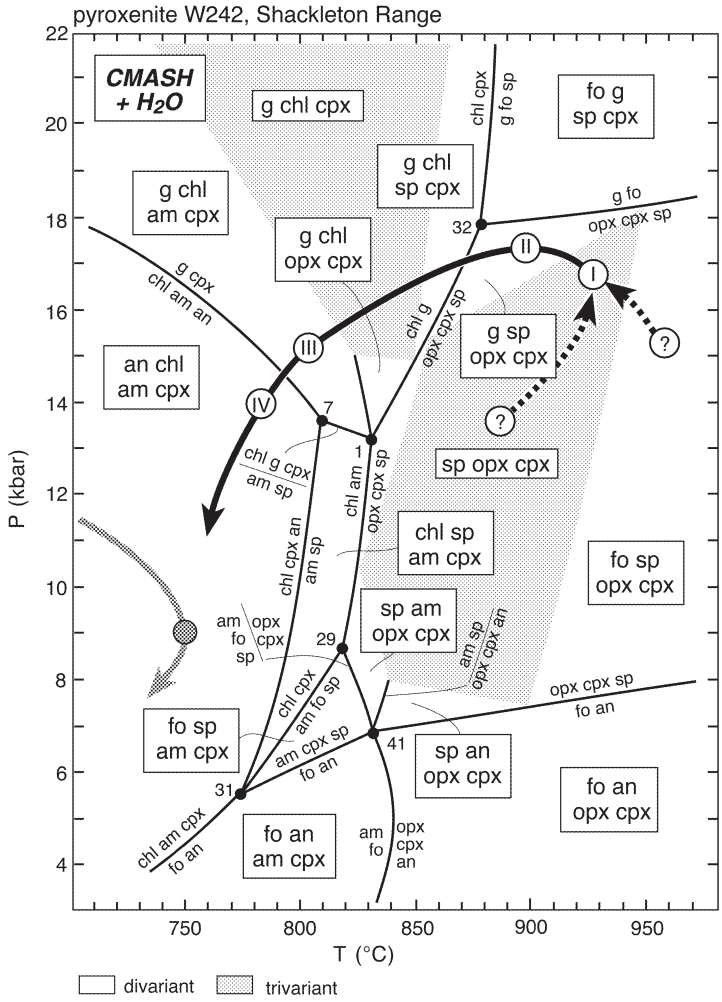

Fig. 11. *P–T* diagram for pyroxenite W242 from the Shackleton Range, Antarctica [composition (in wt %) CaO = 8·5, MgO (+FeO) = 29·0, Al_2O_3 = 15·1, SiO_2 = 38·1], constructed from Fig. 3. The re-equilibration stages I–IV deduced from thin-section observations help to constrain the *P–T* path for the pyroxenite (black). The *P–T* path reconstructed by Schubert & Will (1994) for the granulitic host rock (grey) is given for comparison. Two equilibration stages were distinguished: 660°C and 13·5 kbar (not shown here), and 740°C and 9 kbar (grey circle).

proach of O'Neill & Wood (1979) and O'Neill (1980), and between 890 and 930°C with the calibration by Brey & Köhler (1990).

Implications

This example shows (1) that different assemblages, even in the same type of rock, need not reflect contrasting *P–T* conditions but may stem from bulk-chemical differences, and (2) that the study of chemically different varieties of a rock provides for a more detailed reconstruction of the *P–T* evolution of a tectonic unit. In our example, the phase diagrams proved a valuable instrument to constrain the absolute *P–T* conditions of different re-equilibration stages and, in particular, the overall evolutionary *P–T* trend. In comparison, with conventional thermobarometry alone one *P–T* point around 750–800°C and 7–11 kbar (Marx, 1996) was determined, and no prediction about either the type or shape of the *P–T* path was possible.

The geologic implications of our example are the following. Pyroxenites from the Mount Provender area in the northern part of the Shackleton Range followed an early *P–T* evolution with a high-pressure stage and most probably an anticlockwise *P–T* path not recorded by their host rock granulites and gneisses, for which Schubert & Will (1994) derived a clockwise *P–T* trend and a maximum pressure of 13·5 kbar. These data exclude a shared evolution of both rock types before the host rocks reached their peak metamorphic conditions, which are attributed to the Ross orogeny (Schubert & Will, 1994). Therefore, the emplacement of pyroxenites in their crustal host rocks must have been directly linked with

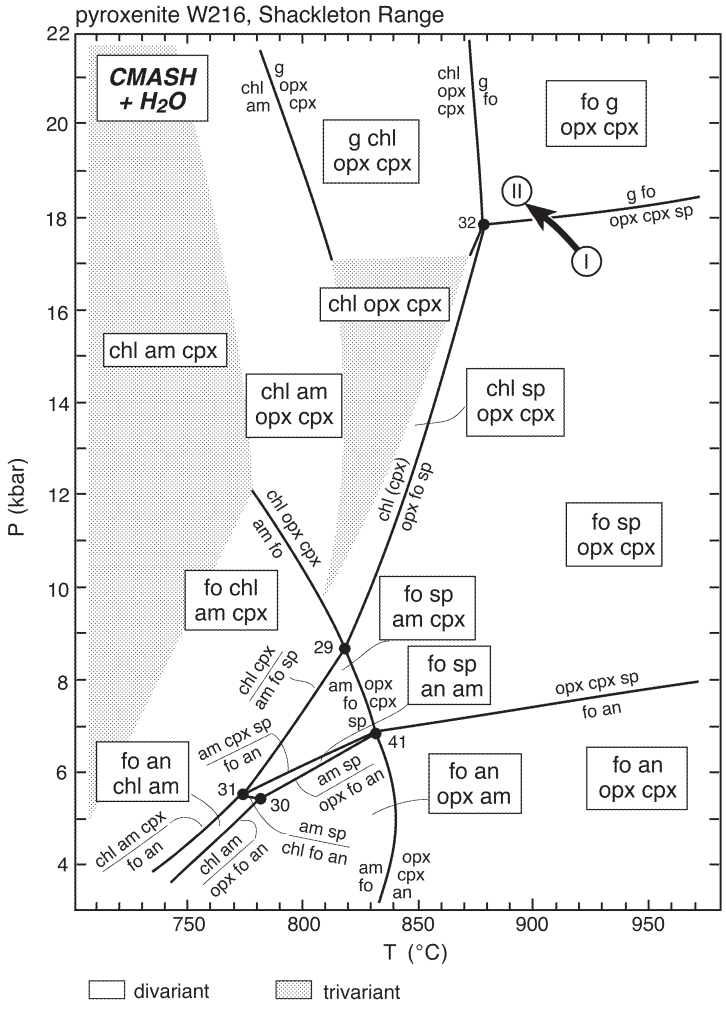

Fig. 12. *P–T* diagram for pyroxenite W216 from the Shackleton Range, Antarctica [composition (in wt %) CaO = 9·6, MgO (+FeO) = 30·8, Al_2O_3 = 6·5, SiO_2 = 47·3], constructed from Fig. 3. The equilibration stages I and II of this pyroxenite point to overstepping the reaction opx + cpx + sp → g + fo as a result of pressure increase. (See also Fig. 10.)

this metamorphic–orogenic event, and occurred most probably during the culmination of crustal thickening or at some stage shortly afterwards.

The pyroxenites give the first evidence of high-pressure metamorphism in the Shackleton Range, deduced from coexisting garnet and olivine. The observed garnet–olivine intergrowths testify to a metamorphic reaction. The preservation of this reaction texture and the failure of textural equilibration in spite of favourable temperature conditions is indication of only a short high-pressure stage within the garnet peridotite field, presumably as a result of rapid tectonic processes. The high-pressure imprint of about 18 kbar can be explained by continent–continent collision, probably in the course of the Ross orogeny, which is thought to be responsible for the emplacement of the ultramafic rocks in their present position. As the surrounding gneiss and granulite record a contrasting *P–T* loop and pressures presumably not exceeding 13·5 kbar (Schubert & Will, 1994), the ultramafic rocks apparently mark a suture zone and imply different tectonic units within the northern Shackleton Range crystalline belt.

In addition, ultramafic rocks are valuable tracers of palaeo-subduction zones. In this context, a recently discovered ophiolite association about 50 km east of the Mount Provender area (Talarico *et al.*, 2000) is particularly interesting. Although the ophiolitic rocks record temperature and pressure conditions (550°C and 7–8 kbar, and 650°C and 5–6 kbar; Talarico *et al.*, 2000) distinctly lower than those of the Mount Provender ultramafics, the ophiolite complex may represent an eastward continuation of the suggested Mount Provender suture zone. However, this must remain speculative until further geological evidence is available and the ophiolitic

character of the Mount Provender ultramafic rocks and their associated amphibolites has been proven.

It is likewise conceivable that the Mount Provender ultramafic rocks represent fragments from the upper mantle that were tectonically 'eroded' during subduction, emplaced in the downgoing lithosphere and involved in the subduction zone, thereby undergoing high-pressure metamorphism. In this case, the Mount Provender rocks may trace a different suture zone than the ophiolites 50 km east. This possibility is supported by the fact that the Mount Provender ultramafic rocks suggest a counterclockwise *P–T* trend. The early *P–T* evolution of pyroxenite with pressure increase can be explained by convergence and lithosphere thickening in the course of the Ross orogeny causing compression, whereas contemporaneous cooling may be the effect of subduction or underplating of relatively cold crustal material. Juxtaposition of hot mantle and cold crustal rocks will lead to further cooling of the former and heating of the latter and, consequently, to convergence of the two *P–T* trajectories. A similar emplacement scenario was suggested for the Erzgebirge, where mantle and crustal rocks reveal similar converging *P–T* paths, only, in this case, both experienced high-pressure metamorphism (Schmädicke & Evans, 1997).

Pyroxenites with basically the same mineral assemblages as in the Mount Provender rocks were reported from the Lanterman Range in North-Victoria Land (Kleinschmidt *et al.*, 1987). As the Lanterman Range pyroxenites also contain the critical assemblage garnet–olivine, a pressure in excess of 18 kbar can be inferred for these rocks. Although speculative, it is possible that the Lanterman Range and the Shackleton Range ultramafics are part of the same subduction system.

There is little doubt that the ultramafic rocks from Mount Provender trace a suture zone, but the reconstruction of palaeo-subduction zones in the Shackleton Range requires more information. Judging from back-arc basin sediments, an early to middle Cambrian south-dipping subduction zone in the northern Shackleton Range was deduced by Kleinschmidt & Buggisch (1994). On the other hand, final collision and southward thrusting of the northern Shackleton Range crystalline belt and a nappe with back-arc sediments over the Read Mountains basement imply a later north-directed subduction zone.

DISCUSSION

Further system components

If a *P–T* path is to be established from the phase diagrams presented here, one has to be aware that these diagrams are constructed for model systems. Natural rocks constitute far more complex chemical systems. Naturally, system components not included in the phase diagrams may influence the phase relations. First, the reaction positions in nature may deviate from those in our model systems and, second, the stability of a phase may be expanded considerably with a further component. The latter happens when a component is strongly fractionated into a particular phase such as, for example, Na in amphibole, whereas plagioclase and clinopyroxene take up only little of this component (Table 3). Of course, any additional component increases the variance of all equilibria.

Chromium

A component behaving in a similar way to Na is Cr. In peridotites, Cr will strongly fractionate into spinel, leading to a further stabilization of spinel in the garnet peridotite stability field. Naturally, the first appearance of garnet with increasing pressure is unaffected by Cr, and, in CMASH, is defined by the univariant reaction opx + cpx + sp → g + fo. In peridotitic bulk compositions, spinel does not occur on the high-pressure side of this reaction, but the CMASH divariant assemblage g–opx–cpx–fo is formed. Theoretically, of course, two different spinel-bearing assemblages are possible on the high-pressure side: g–fo–opx–sp ('seen' by Ca-poor rocks, such as harzburgite) and g–fo–cpx–sp (as in pyroxenite W242), but these are not relevant to an 'average' peridotite (compare Figs 4 and 5).

In the system CMASH–Cr, the above univariant reaction becomes divariant, with all five phases coexisting over a more or less expanded *P–T* field. Thus, as long as there is Cr in the system, spinel does not disappear in peridotites by crossing the above reaction from low to high pressure. With pressure increase, spinel becomes progressively Cr rich, and the pressure at which spinel finally reacts out depends on the Cr content of the system. In an average peridotite, spinel coexists with garnet up to about 25–35 kbar. In refractory, harzburgitic compositions spinel can be stable to much higher pressure. The incorporation of Cr as an additional component in the phase diagram calculations requires the knowledge of the thermodynamic data of at least one further Cr end-member phase, such as knorringite or Cr-Tschermak's pyroxene. As data are rare or not available, it is not possible at present to perform the calculations for a CMASH–Cr model system.

Ferrous iron

Another component to be discussed is ferrous iron. In nature, Fe^{2+} enters any Mg phase to some extent. Because in mantle-derived peridotite, Mg strongly dominates over ferrous iron, and the latter is not much fractionated into a particular Mg–Fe phase, in contrast to Na or Cr, the influence on the phase relations is not severe. Of course,

the variance changes, and all reactions will become divariant assemblages. However, there is no point in including as many system components as possible. In fact, dealing with multicomponent systems other problems arise. For instance, in NCMFASH, the garnet peridotite assemblage g–opx–cpx–fo is quadrivariant and a four-dimensional phase diagram is needed to delineate the phase relations. Of course, with Fe^{2+} added, the reaction positions may deviate to some extent from those in the pure Mg system, but because in nature the effects of Fe and Cr are likely to counterbalance (Evans & Trommsdorff, 1978), CMASH and NCMASH are reasonable model systems to portray the phase relations of Fe-poor, peridotitic rocks.

As pyroxenites commonly are not as Fe poor as mantle peridotites, the reaction positions in natural pyroxenites may deviate somewhat from those in the Fe-free CMASH model system. Hence, a P–T path constructed for a pyroxenite from a CMASH phase diagram does not necessarily give the absolute P–T values. In many cases, however, the relative P–T trajectories are equally conclusive as absolute values if tectonic processes are to be inferred from the paths. In the example of pyroxenite from the Shackleton Range shown here (see above), the P–T conditions predicted by the CMASH phase diagram are in close agreement with conventional thermobarometry on the ol–g–opx–cpx assemblage.

Size of equilibrium domains

The phase diagrams constructed for specific rocks (Figs 4, 6, 7, 9, 11 and 12) were calculated on the assumption that the bulk-rock composition does not change during metamorphism. Apart from compositional changes as a result of the loss or gain of fluid phases, the system chemistry can be modified by changes in the size of the equilibration volume. As equilibration requires diffusion and diffusion is supported by high temperature, the size of the equilibration volumes should become smaller with decreasing temperature. Hence, with the decreasing size of equilibration domains, the actual bulk composition 'participating' in successive mineral reactions in a rock may also change. This is reflected, for example, by porphyroblasts with different core and rim compositions or abundant relic inclusions. In such cases, considerable parts of the original chemical system may be 'sealed up' in large porphyroblasts, thereby being eliminated from the reacting part of the rock volume. These changes in effective bulk composition must be considered if low-temperature rocks or retrograde low-temperature assemblages are concerned and, of course, in case of zoned minerals or porphyroblasts with armoured mineral relics. As this study is focused on peridotite and pyroxenite, dominated by high-temperature assemblages, the equilibration volume can be regarded, in a first approximation, as constant.

Excess water

All the phase diagrams presented are projected from water. This presumption of excess water provides for better comparison of the petrogenetic grids constructed with, for example, the phase diagram of Jenkins (1981) and other experimental results. With an H_2O activity of <1, the positions of dehydration reactions and of involved invariant points are displaced to lower temperature; the pressure position of invariant points remains almost unchanged. The P–T–X data for invariant points in CMASH at $a_{H_2O} = 0{\cdot}5$ are given in Table 2 for comparison.

The assumption of excess water may be more reasonable, in many cases, as it may appear at first. Excess water will cause the rock to stabilize the maximum hydrated assemblage. With the applied calculation method, the modal proportions of phases in assemblages with excess water can be predicted. For example, with the peridotite composition in Fig. 9, the high-pressure assemblage g–am–opx–cpx–fo will contain only about 0–4% calcic amphibole (g: 5–8%, opx: 15–18%, cpx: 6–7%, fo: 67%) at the maximum hydrated state (see isolines of amphibole content in Fig. 9). This, in fact, is an amount not unusual for natural peridotites, for example, for those from the Erzgebirge (Schmädicke & Evans, 1997) or those from Alpe Arami (Schmädicke, unpublished data, 1998). Obviously, only small total quantities of water are required to make a high-pressure peridotite maximum hydrated. Such small amounts of water were apparently present in many Alpine garnet peridotites during metamorphism, and the formation of calcic amphibole during decompression can be explained by 'entering' its stability field rather than by fluid infiltration (Schmädicke & Evans, 1997).

SUMMARY AND CONCLUSIONS

The reliability of calculated equilibria depends on both the quality of thermodynamic data and the choice of appropriate mixing models. The phase diagram calculations for peridotitic and pyroxenitic rocks have shown that ideal molecular mixing models reproduce extremely well both experimentally determined positions of mineral reactions and the compositions of solid solutions suggested from natural rocks. On the other hand, ionic models, which were tested for comparison, proved to be in contrast to nature and experiment. Thus, for the phases and phase components considered (in CMASH and NCMASH), and in the P–T range of interest, ideal

molecular mixing models seem to be a very good approach to reality.

In the case of pyroxenite, the bulk-rock composition has a considerable impact on the phase diagram topology, as the CMASH diagrams for different pyroxenite compositions (Figs 6, 7, 11 and 12) and the SiO_2–Al_2O_3–MgO compatibility diagrams (Fig. 5) reveal. The CMASH grids can only be used for *P–T* estimates if the bulk composition of the pyroxenite in question is close to one of the examples given. There are a few reactions, emanating from invariant point 19 in Fig. 3, that are not strongly susceptible to bulk compositional variations and should, therefore, be seen by many pyroxenites, namely g + cpx = opx + sp + an (i.e. transition from the medium- to the high-pressure granulite facies) and am + sp = opx + cpx + an, or am + sp = opx + cpx + g (e.g. in Figs 6 and 7). However, these reactions are not relevant to SiO_2- and/or Al_2O_3-poor pyroxenites, such as the two examples from the Antarctic (Figs 11 and 12), which are in some instances similar to peridotite.

Some bulk-rock compositions may provide a more complete record of the *P–T* evolution than others. For instance, the pyroxenite from the Erzgebirge (Fig. 7) and sample W242 from the Antarctic (Fig. 11) have a greater potential to 'respond' with changes in the mineral assemblage on a metamorphic *P–T* loop and, thus, provide a finer *P–T* grid than pyroxenite from the Granulitgebirge (Fig. 6) and sample W216 (Fig. 12) from the Antarctic. These contrasting phase diagrams for different pyroxenites exemplify that more than one rock type and more than one sample of each rock type has to be included if a *P–T* path is to be established, as a more detailed picture of the metamorphic evolution can be obtained this way.

The application of the CMASH system to pyroxenite from the Shackleton Range, Antarctica, revealed a high-pressure metamorphic stage around 18 kbar, probably related to continent–continent collision during the Ross orogeny. Furthermore, the sequence of mineral assemblages reconstructed from thin-section observations, combined with the calculated petrogenetic grids, suggests an anticlockwise *P–T* path for the pyroxenite, which is in contrast to the *P–T* evolution in the host rocks. This finding implies a suture zone and, consequently, different tectonic units in the Northern Shackleton Range, and the pyroxenites may trace a palaeo-subduction zone.

The *P–T* diagram in the CMASH model system (Fig. 4) is a reasonably close approximation to the phase relations in peridotites, at least, as long as the stability of calcic amphibole is not concerned. Otherwise, the NCMASH phase diagram in Fig. 9 is the more sophisticated approach, as Na is the component that accounts for the stabilization of calcic amphibole in the garnet peridotite stability field. As stated above, the phase diagram topologies of Figs 4 and 9 will not change with other peridotite compositions, or will change only insignificantly. Within the array of peridotite bulk compositions, the topology of these phase diagrams is not very sensitive to compositional changes. Therefore, the petrogenetic grids presented in this study apply to peridotites in general, and are the first complex quantitative *P–T* diagrams for medium- and high-pressure peridotites, apart from the previous diagram of Jenkins (1981).

ACKNOWLEDGEMENTS

I particularly thank W. Schubert for donating the samples from the Antarctic. Thanks are also due to R. Powell for stimulating discussions, R. Baur and P. Richter for the bulk-chemical analyses, P. Späthe for preparing the thin sections, and to G. Kleinschmidt for providing literature on the Antarctic. I am also indebted to R. Powell, T. Will, and an anonymous referee for their helpful reviews, and especially to M. Wilson for editorial handling. Financial support by Deutsche Forschungsgemeinschaft (Grant Schm 1039/1-1) is gratefully acknowledged.

REFERENCES

Altherr, R. & Kalt, A. (1996). Metamorphic evolution of ultrahigh-pressure garnet peridotites from the Variscan Vosges Mts. (France). *Chemical Geology* **134**, 27–47.

Brey, G. P. & Köhler, T. (1990). Geothermobarometry in four-phase lherzolites. II. New thermobarometers, and practical assessment of existing thermobarometers. *Journal of Petrology* **31**, 1353–1378.

Brey, G. P., Nickel, K. G. & Kogarko, L. (1986). Garnet–pyroxene equilibria in the system CaO–MgO–Al_2O_3–SiO_2 (CMAS): prospects for simplified ('T-independent') lherzolite barometry and an eclogite-barometer. *Contributions to Mineralogy and Petrology* **92**, 448–455.

Buggisch, W., Kleinschmidt, G., Kreuzer, H. & Krumm, S. (1990). Stratigraphy, metamorphism and nappe-tectonics in the Shackleton Range (Antarctica). *Geodätische und Geophysikalische Veröffentlichungen, Reihe I* **15**, 64–86.

Carswell, D. A., Harvey, M. A. & Al-Samman, A. (1983). The petrogenesis of contrasting Fe–Ti and Mg–Cr garnet peridotite types in the high grade gneiss complex of Western Norway. *Bulletin de Minéralogie* **106**, 727–750.

Danckwerth, P. A. & Newton, R. C. (1978). Experimental determination of the spinel peridotite to garnet peridotite reaction in the system MgO–Al_2O_3–SiO_2 in the range 900°–1100°C and Al_2O_3 isopleths of enstatite in the spinel field. *Contributions to Mineralogy and Petrology* **66**, 189–201.

Evans, B. W. & Trommsdorff, V. (1978). Petrogenesis of garnet lherzolite, Cima di Gagnone, Lepontine Alps. *Earth and Planetary Science Letters* **40**, 333–348.

Gasparik, T. (1987). Orthopyroxene thermobarometry in simple and complex systems. *Contributions to Mineralogy and Petrology* **96**, 357–370.

Grew, E. S. & Halpern, M. (1979). Rubidium–strontium dates from the Shackleton Range Metamorphic Complex in the Mount Provender area, Shackleton Range, Antarctica. *Journal of Geology* **87**, 325–332.

Harley, S. L. (1984*a*). The solubility of alumina in orthopyroxene coexisting with garnet in FeO–MgO–Al_2O_3–SiO_2 and CaO–FeO–MgO–Al_2O_3–SiO_2. *Journal of Petrology* **25**, 665–696.

Harley, S. L. (1984*b*). An experimental study of partitioning of Fe and Mg between garnet and orthopyroxene. *Contributions to Mineralogy and Petrology* **86**, 359–373.

Hensen, B. J. (1971). Theoretical phase relations involving cordierite and garnet in the system MgO–FeO–Al_2O_3–SiO_2. *Contributions to Mineralogy and Petrology* **33**, 191–214.

Holland, T. J. B. & Powell, R. (1990). An enlarged and updated internally consistent thermodynamic dataset with uncertainties and correlations in the system K_2O–Na_2O–CaO–MgO–MnO–FeO–Fe_2O_3–Al_2O_3–TiO_2–SiO_2–C–H_2–O_2. *Journal of Metamorphic Geology* **8**, 89–124.

Jenkins, D. M. (1981). Experimental phase relations of hydrous peridotites modelled in the system H_2O–CaO–MgO–Al_2O_3–SiO_2. *Contributions to Mineralogy and Petrology* **77**, 166–176.

Kalt, A., Altherr, R. & Hanel, M. (1995). Contrasting *P–T* conditions recorded in the ultramafic high-pressure rocks from the Variscan Schwarzwald (F.R.G.). *Contributions to Mineralogy and Petrology* **121**, 45–60.

Kleinschmidt, G. & Buggisch, W. (1994) Plate tectonic implications of the structure of the Shackleton Range, Antarctica. *Polarforschung* **63**, 57–62.

Kleinschmidt, G., Schubert, W., Olesch, M. & Reitmann, E. S. (1987). Ultramafic rocks of the Lanterman Range in North Victoria Land, Antarctica, petrology, geochemistry, and geodynamic implications. *Geologisches Jahrbuch, Reihe B* **66**, 232–274.

Marx, I. (1996). Mineralchemie und Phasenpetrologie ultrabasischer Einschaltungen in den Metamorphiten der Haskard Highlands, Shackleton Range, Antarktis. Diploma Thesis, Universität Würzburg, 86 pp.

Medaris, L. G., Jr (1984). A geothermobarometric investigation of the garnet-peridotites in the western Gneiss Region of Norway. *Contributions to Mineralogy and Petrology* **87**, 72–86.

Medaris, L. G., Jr & Carswell, D. A. (1990). Petrogenesis of Mg–Cr garnet peridotites in the European metamorphic belts. In: Carswell, D. A. (ed.) *Eclogite Facies Rocks*. Glasgow: Blackie, pp. 260–290.

Morten, L. & Obata, M. (1983). Possible high-temperature origin of pyroxenite lenses within garnet peridotite, northern Italy. *Bulletin de Minéralogie* **106**, 775–780.

Nixon, P. H. (1987). *Mantle Xenoliths*. Chichester: John Wiley.

Obata, M. & Morten, L. (1987). Transformation of spinel lherzolite to garnet lherzolite in ultramafic lenses of the Austridic Crystalline Complex, Northern Italy. *Journal of Petrology* **28**, 599–623.

Obata, M. & Thompson, A. B. (1981). Amphibole and chlorite in mafic and ultramafic rocks in the lower crust and upper mantle. *Contributions to Mineralogy and Petrology* **77**, 74–81.

O'Neill, H. S. C. (1980). An experimental study of the Fe–Mg partitioning between garnet and olivine and its calibration as a geothermometer: corrections. *Contributions to Mineralogy and Petrology* **72**, 337.

O'Neill, H. S. C. (1981). The transition between spinel lherzolite and garnet lherzolite, and its use as a geobarometer. *Contributions to Mineralogy and Petrology* **77**, 185–194.

O'Neill, H. S. C. & Wood, B. J. (1979). An experimental study of the Fe–Mg partitioning between garnet and olivine and its calibration as a geothermometer. *Contributions to Mineralogy and Petrology* **70**, 59–70.

Pawley, A. R. & Holloway, J. R. (1993). Water sources in subduction zone volcanism: new experimental constraints. *Science* **260**, 664–667.

Powell, R. (1985). Regression diagnostics and robust regression in geothermometer/geobarometer calibration: the garnet–clinopyroxene geothermometer revisited. *Journal of Metamorphic Geology* **3**, 231–243.

Powell, R. & Holland, T. J. B. (1988). An internally consistent thermodynamic dataset with uncertainties and correlations. 3. Applications to geobarometry, worked examples and a computer program. *Journal of Metamorphic Geology* **6**, 173–204.

Powell, R., Holland, T. & Worley, B. (1998). Calculating phase diagrams involving solid solutions via non-linear equations, with examples using THERMOCALC. *Journal of Metamorphic Geology* **16**, 577–588.

Schmädicke, E. & Evans, B. W. (1997). Garnet-bearing ultramafic rocks from the Erzgebirge, and their relation to other settings in the Bohemian Massif. *Contributions to Mineralogy and Petrology* **127**, 57–74.

Schubert, W. & Will, T. (1994). Granulite-facies rocks from the Shackleton Range, Antarctica. Conditions of formation and preliminary petrogenetic implications. *Chemie der Erde* **54**, 355–371.

Talarico, F., Kleinschmidt, G. & Henjes-Kunst, F. (2000). An ophiolitic complex in the northern Shackleton Range, Antarctica. *Terra Antarctica* (in press).

Will, T. M. (1998). *Phase Equilibria in Metamorphic Rocks*. Berlin: Springer.

Will, T. M., Powell, R., Holland, T. J. B. & Guiraud, M. (1990). Calculated greenschist facies mineral equilibria in the system CaO–FeO–MgO–Al_2O_3–SiO_2–CO_2–H_2O. *Contributions to Mineralogy and Petrology* **104**, 353–368.

Wilson, M. (1989). *Igneous Petrogenesis*. London: Harper Collins Academic.

Zhang, R. Y., Liou, J. G. & Cong, B. L. (1995). Talc-, magnesite- and Ti-clinohumite-bearing ultrahigh-pressure meta-mafic and ultramafic complex in the Dabie Mountains, China. *Journal of Petrology* **36**, 1011–1037.